www.czasopisma.pan.pl PAN POLSKA AKADEMIA NAUK www.journals.pan.pl

Arch. Min. Sci. **69** (2024), 4, 655-674

Electronic version (in color) of this paper is available: http://mining.archives.pl

DOI: https://doi.org/10.24425/ams.2024.152579

GUOZHEN ZHAO[1,2*], FENGYI CHANG[1], SHUAI WANG[1]

MECHANICAL BEHAVIOUR OF FRACTURE LAYER FAILURE IN SECONDARY MINING COMPOSITE ROOF STRATA

In the extremely close distance of lower coal seam mining, affected by secondary mining, the fractures expand through the layer in the composite roof, and this process is complex and diverse. In this paper, a three-point bending load test of different strength rocks and their combinations is conducted by combining acoustic emission. The results indicate that the overall deflection angle in the lower roof is approximately 8° smaller than that in the upper roof. When the fracture extends from the brittle roof to the plastic roof, the deflection angle in both types of roofs increases. When the plastic roof extends to the brittle roof, the deflection angle of the brittle roof increases while that of the plastic roof decreases. The damage degree of the composite rock mass during the failure process lies between the two single rock masses that make up the composite rock mass. The damage is dense at the initial expansion moment of the fracture in the rock mass, but weak when the interface expands through the layer. The energy evolution of the composite roof mainly depends on the high-strength roof, and the horizontal migration process of the fracture at the interface does not release energy.

Keywords: Secondary mining; composite roof; fracture wear layer; deflection angle; acoustic emission characteristics

1. Introduction

In recent years, as coal mining intensity continues to increase, the single coal seam with better occurrence conditions has been increasingly depleted, and most mines are facing close coal seam mining [1]. In the close distance coal seam of longwall mining, the mining of the upper coal seam breaks the stress balance state of the stope. The roof of the coal seam forms a complex

[1] TAIYUAN UNIVERSITY OF TECHNOLOGY, COLLEGE OF MINING ENGINEERING, 030024, TAIYUAN, CHINA
[2] TAIYUAN UNIVERSITY OF TECHNOLOGY, KEY LABORATORY OF IN-SITU PROPERTY-IMPROVING MINING OF MINISTRY OF EDUCATION, 030024, TAIYUAN, CHINA

* Corresponding author: zhaoguozhen@tyut.edu.cn

fracture network [2,3]. During the mining process of the lower coal seam, the roof is affected by secondary mining, resulting in more intense mine pressure and more intensive roof fractures [4,5]. This will increase the possibility of disasters such as roof fall [6], mine air leakage [7,8], and mine water inrush [9], which brings serious safety problems to the efficient mining of coal mines. According to the theory of 'masonry beam' [10], in the process of close upper coal seam mining, with the advancement of the working face, the rock layer between the two layers of coal is broken and collapsed by mining disturbance, and the key stratum is broken to form a 'masonry beam' structure, as shown in Fig. 1.

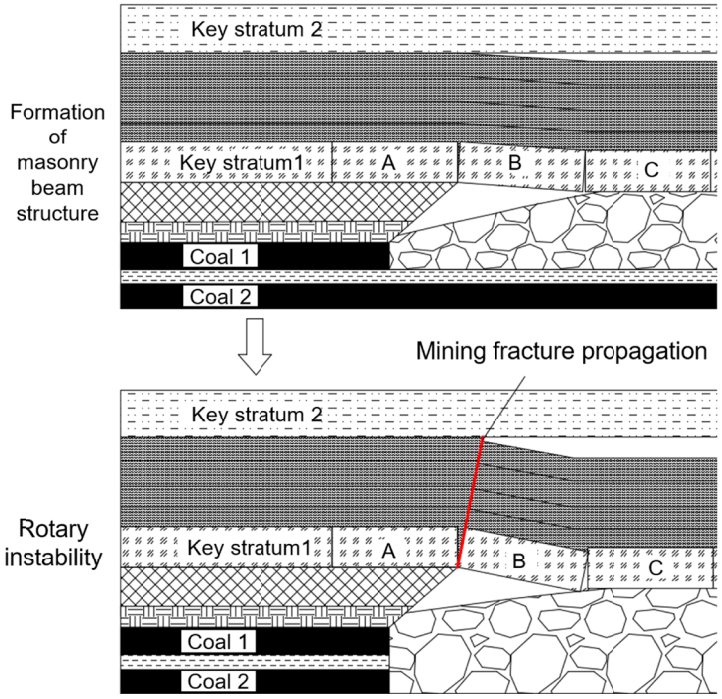

Fig. 1. Close distance coal seam mining

As shown in Fig. 1, during the extraction of the lower coal seam, key block C continues to subside with the collapsing rock, while key block B undergoes rotational deformation, which may lead to rotational instability. If the masonry beam structure experiences rotational instability, the soft rock above key block B will also collapse, causing mining-induced fractures to propagate upward along the inclined roof. The roof of the working face is composed of rock strata with different lithology, and its failure behaviour is complex and diverse. The study of the mechanical behaviour of the fracture layer failure in the combined rock can reflect the fracture propagation law of the composite roof strata, which has crucial engineering significance.

Scholars have carried out a lot of research on the influence of secondary mining on the stope and the failure of rock fractures through the layer [11-15]. Zhang analysed the distribution pattern of mining-induced fractures in the process of coal seam mining using field drilling exploration

and theoretical calculation. The research shows that under the condition of repeated mining, the fracture zone extends to the coal pillars on both sides of the working face, and the fractures on both sides of the working face are significantly higher than those in the middle of the working face. An 'M'-shaped fracture distribution pattern is formed in the overlying rock [16]. Li used the method of similar material simulation experiments and theoretical analysis to analyse the evolution law of overburden rock fracture under the condition of single coal seam mining and superimposed mining. The results show that the overburdened rock collapse, mine pressure behaviour and fracture development of upper coal seam mining are the same as those of single coal seam mining. After the mining of the lower coal seam, the equilibrium state of the overburdened rock collapse structure of the upper coal seam is destroyed under the influence of superimposed mining, and a large number of fractures are developed [17]. Cao et al. made specimens of prefabricated fractures and studied the fracture coalescence mechanism by changing the angle of prefabricated fractures relative to the loading direction and spacing. It is concluded that the interaction of multiple fractures leads to the continuous degradation of the macroscopic mechanical properties of rock mass, weakens the relative sliding trend of coplanar fractures, and changes the coalescence mode of specimens [18]. Wang et al. used ABAQUS to carry out numerical simulation experiments on single-layer layered rock mass with different thicknesses of prefabricated fractures. It was concluded that under different thickness conditions, the bedding plane shows the effect of preventing the fracture from expanding upward. At the same time, the fracture propagation in the layered rock mass is discontinuous, and the fracture tip migrates horizontally along the bedding plane, showing a stepped shape as a whole [19]. Yang et al. analysed the characteristics of layered rock fracture propagation by DSCM (Digital Speckle Correlation Method), acoustic emission and numerical simulation based on the three-point bending test of different rock combinations. The research shows that rock strength, bedding plane strength and pre-existing fracture position are all crucial factors affecting fracture propagation [20]. Wang et al. combined with DIC (Digital Image Correlation) technology to study the peak strength and failure characteristics of 45 kinds of rock mass with double prefabricated fractures. The research shows that when the fracture inclination angle reaches 45°, the total length of the fracture is the longest, and the effect of the prefabricated fracture combination is the best. Except for the specimen with a fracture inclination angle of 90°, the other types of fractures expand and penetrate near the lower part of the specimen [21]. Chen conducted three-point bending tests on rock specimens with prefabricated notches at different angles. The study revealed that fracture inclination and changes in lithology are key factors influencing the stability of roadway roofs [22]. Lin combined acoustic emission technology with three-point bending tests on layered sandstone to analyse the failure patterns of roadway sandstone roofs. The experimental results indicated that specimen strength and deformation are linearly positively correlated with specimen height and linearly negatively correlated with span [23]. Yang et al. conducted three-point bending tests and numerical simulations on both single and combined sandstone specimens, using digital image correlation and acoustic emission techniques to investigate the crack propagation process. The results showed that, in addition to rock layer strength, the main factors influencing crack propagation include bedding plane strength and the location of pre-existing fractures [24].

The above literature mainly studies the influence of secondary mining on the fracture in the stope and the expansion law of fractures in the layered rock mass. However, there are few studies on the law of the fracture of secondary mining composite roof strata by experimental means. This study utilises acoustic emission monitoring technology and employs a testing machine to con-

duct three-point bending load tests on rocks of varying strengths and their combinations. The research analyses the fracture propagation patterns induced by notches in different rock types, the 'load-displacement' curve characteristics during testing, and the acoustic emission properties of the rocks. By investigating the mechanical behaviour of roof strata failure, inter-layer fracture propagation, and energy evolution under the influence of secondary mining, the study identifies the fracture propagation patterns during roof pressure events. These findings facilitate roof management during pressure events and are of great significance for mine disaster warning and control, as well as for water-preserving and environmentally friendly mining.

2. Test Equipment and programs

Three-point bending test can simulate the whole process of rock failure under tensile stress. To investigate the mechanical failure behaviour and inter-layer fracture propagation patterns of composite roof strata in close-distance coal seams under the influence of secondary mining, three-point bending load tests were carried out on different strength rocks and their combinations with prefabricated notches. Prefabricated notches were used to simulate the damage caused by primary mining to rock mass. Combined with acoustic emission, the 'load-displacement' curve, failure mode and acoustic emission characteristics during the test were analysed, and the propagation law of fractures under secondary mining was obtained.

2.1. Specimen preparation

The three-point bending test includes three groups of rock samples: tensile strength test group, single rock three-point bending group and composite rock three-point bending group. The parameters of the rock samples are presented in TABLE 1.

TABLE 1

Rock sample parameters required for the test

Serial number	Group	Rock properties	Size / mm	Number of samples	Remark
1	Tensile strength test group	Fine sandstone	Φ50×30	3	Brazilian splitting test
2		Limestone	Φ50×30	3	
3		Mudstone	Φ50×30	3	
4	Three-point bending group of single rock	Fine sandstone	100×50×50	3	
5		Limestone	100×50×50	3	
6		Mudstone	100×50×50	3	
7	Three-point bending group of composite rock	Limestone (lower) – mudstone (upper)	100×50×50	3	Fissure from strong to weak
8		Mudstone (lower) – fine sandstone (upper)	100×50×50	3	
9		Fine sandstone (lower) – mudstone (upper)	100×50×50	3	Fissure from weak to strong
10		Mudstone (lower) – limestone (upper)	100×50×50	3	

The test samples of the single rock three-point bending group were prefabricated with notches of 5 mm in length by wire cutting in the middle of the bottom. Fig. 2 presents the test samples of the three-point bending group of the combined rock, which is composed of two rocks of the same volume and different lithology. The rocks are bonded with marble glue with a thickness of less than 1 mm. The notches with a length of 5 mm are prefabricated in the middle of the bottom of each sample by wire cutting.

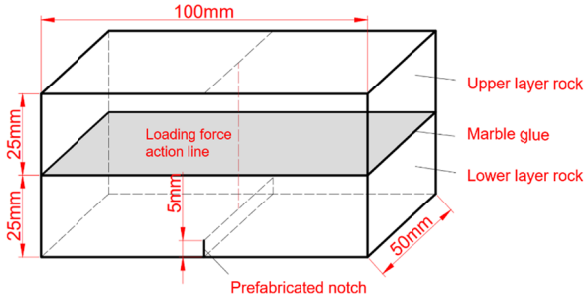

Fig. 2. Shape diagram of rock combination

2.2. Rock tensile strength test

The maximum tensile stress that the rock can withstand when it reaches failure under uniaxial tension is called the uniaxial tensile strength of the rock. The Brazilian splitting test is a tensile strength test method recommended by the rock mechanics test procedure and belongs to the indirect tensile test. The Brazilian splitting test was carried out on the samples of the tensile strength test group by using the testing machine. The maximum pressure of each disc sample was obtained, and the tensile strength of the corresponding rock was obtained. The data is presented in TABLE 2.

TABLE 2

Brazilian rock splitting test results table

Sample	Numbering	Measured sample size / mm		Maximum force of rock failure / kN	Determination of tensile strength / MPa
		Diameter	Height		
Fine sandstone (Φ50×30)	1-1	48.56	29.52	6.83	3.03
	1-2	49.00	30.00	5.77	2.50
	1-3	49.18	31.32	7.82	3.24
	Average value				2.92
Limestone (Φ50×30)	2-1	49.24	30.60	21.05	8.90
	2-2	49.56	29.58	21.53	9.35
	2-3	49.80	30.52	22.78	9.55
	Average value				9.27
Mudstone (Φ50×30)	3-1	49.70	30.80	16.03	6.67
	3-2	49.28	27.16	14.04	6.68
	3-3	49.36	31.22	16.21	6.70
	Average value				6.68

It can be concluded from the data in TABLE 2 that the uniaxial tensile strength of the three rocks from weak to strong is fine sandstone, mudstone and limestone. Their average uniaxial tensile strength ratio is 1:2.3:3.2.

2.3. Three-point bending test equipment and scheme

2.3.1. Three-point bending test equipment

The three-point bending test equipment consists of a loading system, an acoustic emission system and a camera system (Fig. 3). The loading system controls the testing machine to apply pressure on the sample through the laboratory computer and records load, displacement, time and other data in real-time at the PC end. The acoustic emission system records the basic acoustic emission parameters through sensors placed on the surface of the sample to obtain the acoustic emission characteristic information during the test. The camera system uses a digital camera to shoot the front of the sample to obtain the fracture characteristics of the sample surface during the test.

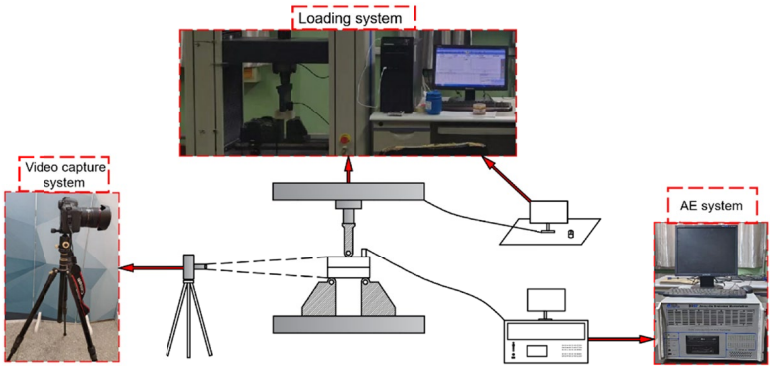

Fig. 3. Three-point bending test device

2.3.2. Three-point bending test scheme

(1) Install the three-point bending mould on the test machine, adjust the span between the lower two fulcrums to 80 mm, and put the rock sample between the moulds.
(2) Connect the acoustic emission system. The acoustic emission sensor is fixed in a smooth place on the upper right of the specimen to ensure the stability of the sensor during the test. The contact surface between the sensor and the specimen is smeared with a vaseline coupling agent to make the two full contacts. Open the acoustic emission supporting software on the PC side and set the acoustic emission acquisition parameters.
(3) Debugging the camera system. Firstly, install the camera on the levelling tripod. Then, adjust the height of the camera to make it at the same height as the sample. Finally, adjust the camera focal length, image file format, image storage location and other related parameters.
(4) Starting the testing machine, use the loading method of axial displacement control to preload the sample at a rate of 0.01 mm/s until the load reaches 0.1 kN. Then, transfer

the testing machine to the formal loading mode and start the acoustic emission system and the camera system synchronously. The test ends when the fractures on the surface of the sample expand and run through the entire sample. In the process of formal loading, the test machine still adopts the loading method of displacement control, with a loading rate of 0.001 mm/s. In this test, three systems need to be controlled by different personnel to ensure the synchronous acquisition of data during formal loading.

(5) Save all kinds of data collected during the test, remove the acoustic emission probe on the surface of the specimen, replace the sample, and carry out the next set of tests.

3. Propagation law of secondary mining fracture in single rock

The prefabricated notches at the bottom of the single rock sample simulate the fractures generated by the roof after the first mining of the close-distance coal seam. By applying the load to the sample, the expansion morphology and acoustic emission characteristics of the fractures when the single rock is destroyed are analysed, and the fracture propagation law of the single roof rock layer under the secondary mining is obtained.

3.1. Characteristics of 'load-displacement' curve of single rock under three-point bending

There are great differences in the trend of 'load-displacement' curves of different single rocks under three-point bending, and there are also some commonalities. Fig. 4 presents the 'load-displacement' curves of rocks with different strengths.

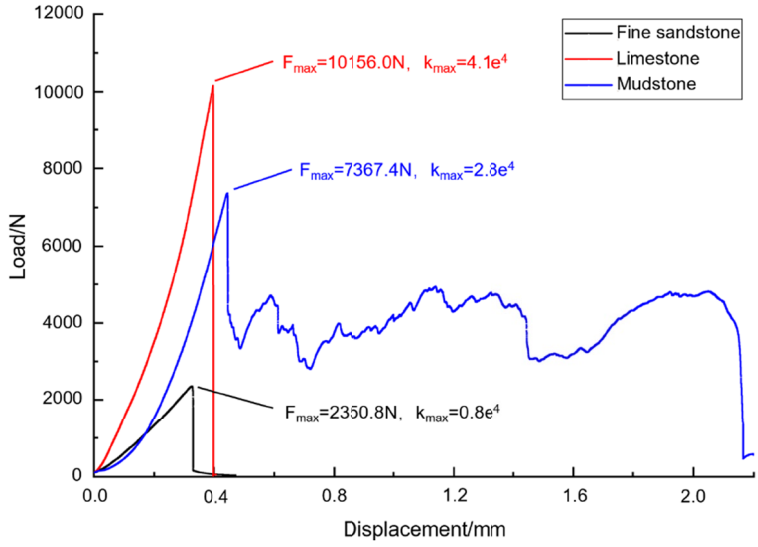

Fig. 4. Load-displacement' curves of rocks with different strengths

It can be seen from Fig. 4 that under the action of three-point bending, the 'load-displacement' curves of the three rocks have the following characteristics:

(1) The 'load-displacement' curves of the three kinds of rocks are approximately linear growth in the early stage of loading, and approximately vertical decline after reaching the peak load. The relationship between the slope of the linear growth stage and the peak load is fine sandstone < mudstone < limestone, which is consistent with the relationship between the uniaxial tensile strength of the three kinds of rocks presented in TABLE 2.

(2) Compared with fine sandstone and limestone, there is residual stress in the fracture propagation stage of mudstone. The 'load-displacement' curve of this stage is complex and shows post-peak bearing characteristics. However, the 'load-displacement' curve of limestone and fine sandstone has no obvious fracture propagation stage, and the peak load of limestone is higher than that of fine sandstone. Therefore, both limestone and fine sandstone are brittle rocks, and the brittleness of limestone is stronger than that of fine sandstone, while mudstone is plastic rock.

3.2. Propagation law of secondary mining fracture in single rock

In the process of applying the load, the fractures generated by the prefabricated notch at the bottom of the specimen begin to expand from the top. Due to the anisotropy of the rock, fractures will deflect to varying degrees and continue to expand to the top of the specimen until the specimen is destroyed. Fig. 5 presents the failure modes of three specimens in each group of a single rock. The red in the figure is marked as the overall deflection angle of the fracture, that is, the angle between the line between the initial point and the end point of the fracture expansion and the vertical direction. The blue in the figure is marked as the maximum deflection angle of the fracture, that is, the maximum angle between the expansion direction and the vertical direction during the fracture expansion process. By analysing the variation characteristics of these two angles during the fracture expansion process, the expansion law of the secondary mining fracture of a single rock is obtained.

Fig. 5 shows that the new fracture of fine sandstone initiates at the top of the prefabricated notch and expands upward along the prefabricated notch. The range of the maximum deflection angle during fracture propagation is 20-24°, and the overall deflection angle range of the fracture is 1-5°. The new fracture of limestone also initiates at the top of the prefabricated notch and expands upward along the prefabricated notch. The range of the maximum deflection angle during the fracture propagation is 18-26°, and the overall deflection angle range of the fracture is 0-2°. The new fracture initiation position of mudstone will deviate from the prefabricated notch. The maximum deflection angle during the fracture propagation process is 66-75°, and the overall deflection angle of the fracture is 9-25°.

Comparing Fig. 5(a) and Fig. 5(b), it is clear that the new fractures of brittle rocks will begin to expand at the top of the prefabricated notches. Moreover, the higher the tensile strength of the rock, the smaller the deflection amplitude during the fracture propagation process, and the overall fracture tends to be more linear. This phenomenon shows that under the action of secondary mining, the secondary mining fracture of a single brittle roof will initiate at the top of the existing fracture and expand along the original fracture. The higher the uniaxial tensile strength of the single brittle roof, the smaller the dispersion degree of the secondary mining fracture expansion.

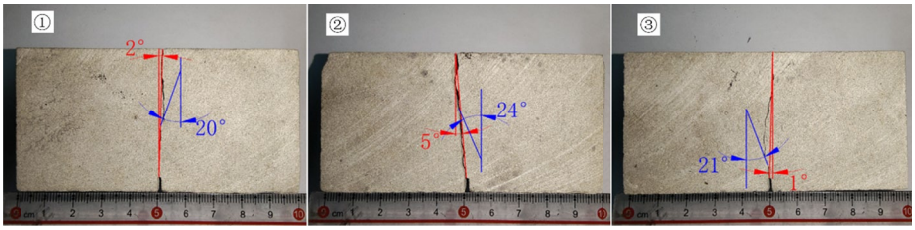

(a) Failure pattern of fine sandstone

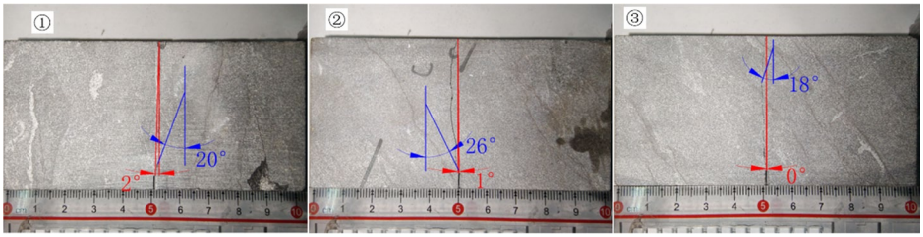

(b) Failure pattern of limestone

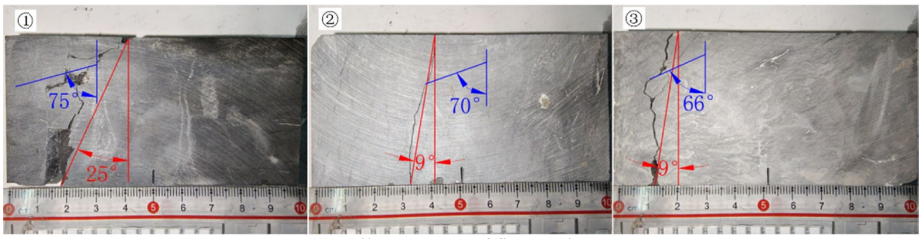

(c) Failure pattern of fine mudstone

Fig. 5. Three-point bending test failure pattern of single rock

By comparing Fig. 5(a), Fig. 5(b) and Fig. 5(c), it can be seen that the new fracture initiation position of mudstone shows randomness and the deflection amplitude in the process of fracture propagation increases significantly, which is different from that of single brittle rock. This phenomenon shows that under the action of secondary mining, the secondary mining fracture of a single plastic roof does not necessarily expand along the top of the primary mining fracture, and the deflection of the secondary mining fracture is larger than that of the brittle rock.

3.3. Secondary mining failure behaviour and energy characteristics of single rock

The cumulative acoustic emission count can reflect the total amount and frequency of the formation and expansion of fractures inside the specimen. The absolute energy can truly reflect the impact signal energy inside the specimen during the test and can reflect the scale of the internal fracture of the rock. The corresponding relationship between the cumulative acoustic emission count, absolute energy and load of a single rock under three-point bending is shown in Figs. 6 to 8.

Fig. 6 shows that during the loading process of fine sandstone, the cumulative acoustic emission count continuously increases before the peak load. Tiny fractures inside the sample are compacted, and new microfractures are generated. In this process, the cumulative acoustic emission

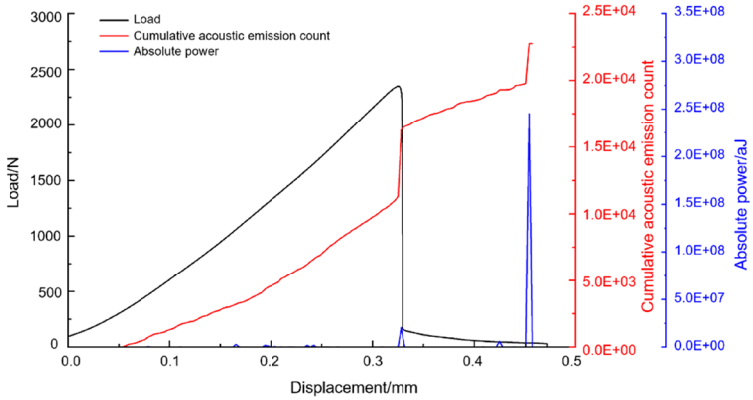

Fig. 6. Three-point bending 'load-cumulative acoustic emission count-absolute energy-displacement' curve of fine sandstone

count reaches 1.1×10^4. At the peak load, the fractures expand instantaneously, and macroscopic fractures appear. The acoustic emission signal is strong and accompanied by significant energy release. The cumulative acoustic emission count increases by 5.0×10^3, and the absolute energy released reaches 2.0×10^7 aJ. After the peak load, with the expansion of the fracture, the cumulative acoustic emission count continues to rise, increasing by 3.5×10^3. At the moment when the fracture penetrates the fine sandstone, the cumulative acoustic emission count increases sharply again, and the released energy reaches the peak. The cumulative acoustic emission count increases by 3.0×10^3, and the absolute energy peak is 2.5×10^8 aJ. The rock is destroyed at this time. The above rules show that fine sandstone has an energy absorption effect. This is due to its large particles. In the early stage of loading, the fractures between particles are compacted, which can accommodate a certain amount of deformation. The growth of the acoustic emission count and the release of absolute energy at the two key time points of the initial fracture propagation and the fracture penetration specimen are the most obvious, and the fracture propagation speed is the fastest.

Fig. 7 shows that in the initial stage of limestone loading, only a small amount of acoustic emission counts appeared, and the cumulative acoustic emission count was only 685. At this time, limestone almost did not produce damage. In the middle of loading, the 'load-displacement' curve of limestone is slightly concave downward, and the micro-fractures in limestone are gradually generated. At this time, the acoustic emission signal begins to be active, and the cumulative acoustic emission count gradually increases, with an increment of 1.3×10^4. When the load reaches the peak load, the fracture penetrates the specimen. Limestone is destroyed in an instant, and the bearing capacity is lost. The acoustic emission signal is strong, and the cumulative acoustic emission count increases by 8.7×10^4 and reaches the maximum value. Limestone only shows an obvious energy peak at the peak load, and the absolute energy peak is 1.5×10^9 aJ. Almost no energy is released in the other stages. The above acoustic emission law shows that limestone is dense, brittle and high strength. There is almost no damage to limestone in the early stage of loading. When the maximum bearing capacity is reached, it is destroyed at once, releasing a lot of energy, which is manifested as severe roof pressure.

Fig. 8 shows that in the early stage of mudstone loading, the acoustic emission signal is more active. The cumulative acoustic emission count continues to rise, and the tiny fractures in the

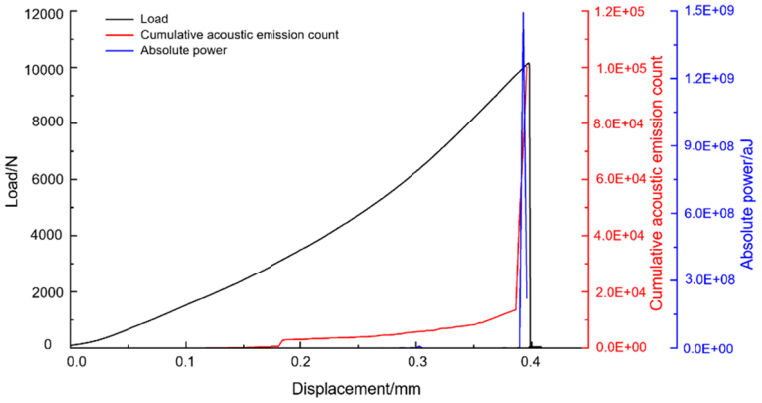

Fig. 7. Three-point bending 'load-cumulative acoustic emission count-absolute energy-displacement' curve of limestone

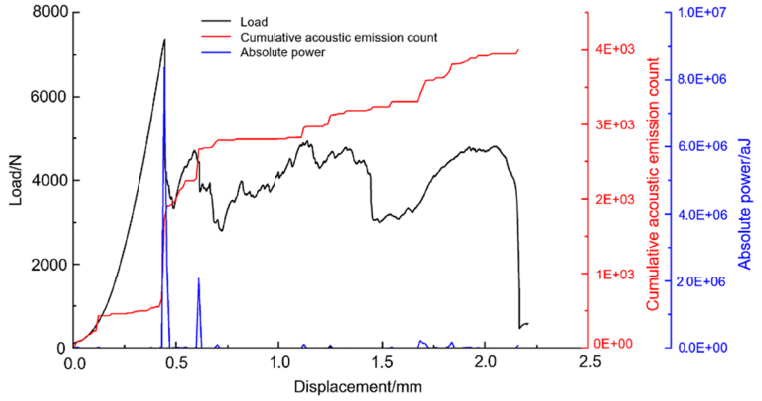

Fig. 8. Three-point bending 'load-cumulative acoustic emission count-absolute energy-displacement' curve of mudstone

mudstone are gradually compacted. The cumulative acoustic emission count reaches 432. After the internal fractures of the mudstone are compacted, they are shown as elastomers. The cumulative acoustic emission count is stable, and the acoustic emission count increment is 120. The mudstone is in a relatively stable state in a short time. When loaded to the peak load, macroscopic fractures appear on the surface of the mudstone. The acoustic emission signal of mudstone is active, and the cumulative acoustic emission count increases by 1.7×10^3. After the peak load, the macroscopic fractures of mudstone continue to expand with the loading. The cumulative acoustic emission count shows a step-by-step cycle of 'stable growth'. When the mudstone is destroyed, the cumulative acoustic emission count reaches a maximum of 4.0×10^3. The energy released by mudstone at the peak load is the largest, and the absolute energy peak is 8.4×10^6 aJ. After that, there are several insignificant energy releases in the fracture propagation stage. The above acoustic emission law shows that the mudstone is plastic and contains more primary fractures. The primary fractures are compacted in the early stage of loading and have an energy absorption effect.

The energy released by mudstone at the initial expansion moment of fracture is the largest. At the same time, mudstone has a certain residual strength after failure and still has bearing capacity.

The following rules can be obtained by analysing Figs. 6 to 8:

(1) The load of the three kinds of rocks in the three-point bending test is consistent with the change of acoustic emission signal. The load curve is approximately linear growth to the peak load and then drops sharply in the early stage. The cumulative acoustic emission count shows an overall growth trend and increases sharply at the peak load.

(2) The cumulative acoustic emission count of rock under three-point bending in descending order is limestone > fine sandstone > mudstone. The displacement required for complete failure of rock under three-point bending in ascending order is limestone < fine sandstone < mudstone. The above rules show that under the action of secondary mining, the stronger the brittleness of the roof, the more internal damage there is and the more complete the damage. The failure process of the brittle roof is short, while the failure process of the plastic roof is long, which indicates that the failure process of the plastic roof is more moderate than that of the brittle roof.

(3) The energy release in the failure process of brittle roofs is concentrated, while that of plastic roofs is dispersed. The energy released by the brittle roof is the largest when the final fracture occurs, and the energy released by the plastic roof is the largest when a fracture occurs.

(4) The total absolute energy released by fine sandstone is 3.0×10^8 aJ, that released by limestone is 1.8×10^9 aJ, and that released by mudstone is 1.4×10^7 aJ. The above data show that the higher the tensile strength of the brittle roof, the more energy is released during the fracture process. The energy released during the fracture process of the brittle roof is higher than that released during the fracture process of the plastic roof.

4. The propagation law of secondary mining fractures in composite rock

The notch at the bottom of the combined rock sample is prefabricated in the same way as that of the single rock, to simulate the fracture generated by the roof of the coal seam after the first mining of the close-distance coal seam. By applying the load to the sample, the expansion form and acoustic emission characteristics of the combined rock fracture in the process of crossing the layer are analysed , and the law of the fracture crossing the layer of the roof rock layer under the secondary mining is studied.

4.1. ‘Load-displacement’ curve characteristics of composite rock under three-point bending

The ‘load-displacement’ curves of rocks with different strength combinations are compared, as shown in Fig. 9.

It can be seen from Fig. 9 that the ‘load-displacement’ curves of rocks with different strength combinations under three-point bending will show different characteristics. In general, there will be two peak loads in the combined rock during the three-point bending load, which is a bimodal curve, and the first peak load is less than the second peak load. The first ‘up-down’ change of

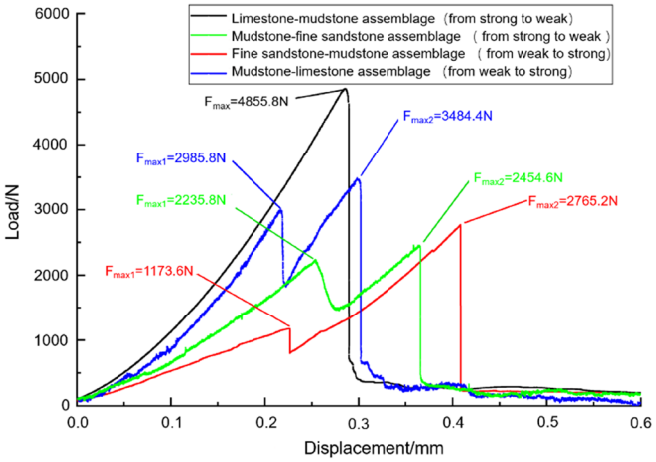

Fig. 9. The 'load-displacement' curves of rocks with different strength combinations

the load represents the expansion process of the fracture in the lower rock, and the second 'up-down' change of the load represents the process of the generation and expansion of the upper rock fracture. When the strength of the lower rock in the composite rock is much larger than that of the upper rock, the high stress generated by the fracture of the lower rock will cause the upper rock to fracture at the same time, and the fracture will expand to the upper rock instantaneously, resulting in only one peak load in the three-point bending load process of the composite body, showing a single peak curve. Comparing Fig. 4 and Fig. 9, it can be seen that the peak load of the single rock in the composite roof is less than that of the single rock.

4.2. The propagation law of secondary mining fractures in composite rock

In the process of applying load, the prefabricated notches at the bottom of the specimen begin to expand from its top. When the fractures expand to the interface of the two layers of rock, they will migrate horizontally at the interface for a certain distance. New fractures will sprout in the lower part of the upper rock and continue to expand upward until the specimen is completely destroyed. Fig. 10 presents the failure mode of the specimen. The red colour is marked as the expansion form of the fracture, the blue colour is marked as the deflection angle of the whole fracture, that is, the angle between the connection line and the vertical direction between the initial point and the end point of the fracture expansion. By analysing the variation characteristics of the overall deflection angle in the process of fracture expansion, the secondary mining expansion law of the fracture of the combined rock is obtained.

According to Fig. 10, when the secondary mining fracture expands from high-strength rock to low-strength rock, the average deflection angle in high-strength rock is 11.8°, and the average deflection angle in low-strength rock is 19.5°. When the secondary mining fracture expands from low-strength rock to high-strength rock, the average deflection angle in low-strength rock is 9.5°, and the average deflection angle in high-strength rock is 17.7°. The above data show that when the secondary mining fracture expands in different strength rock combinations, the

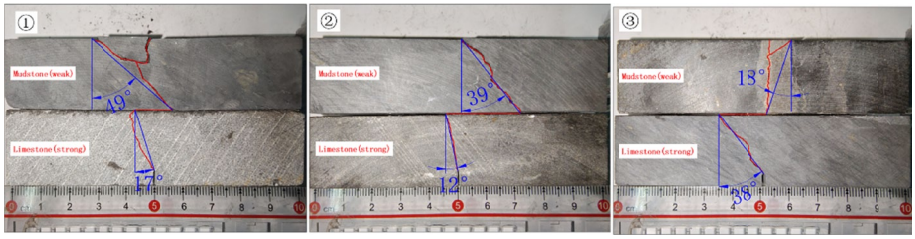

(a) Limestone-mudstone failure pattern

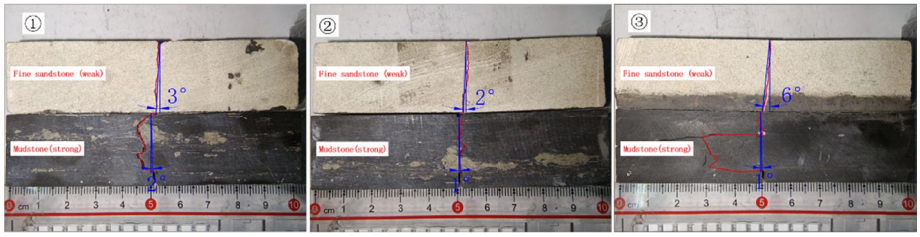

(b) Mudstone-fine sandstone failure pattern

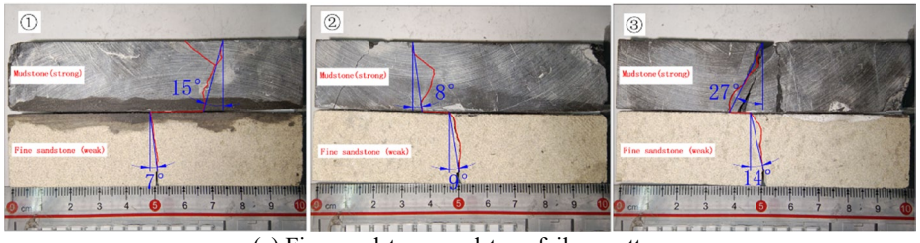

(c) Fine sandstone-mudstone failure pattern

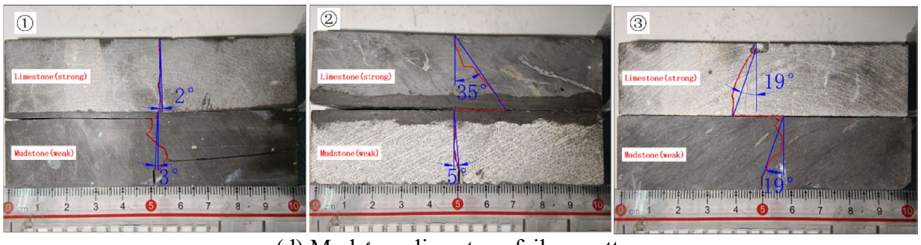

(d) Mudstone-limestone failure pattern

Fig. 10. Three-point bending test failure pattern of composite rock

deflection angle of the fracture in the lower rock is smaller than that in the upper rock. The average deflection angle difference between the two layers of rock is about 8°. This is because the new fracture of the lower rock begins to expand from the tip of the prefabricated notch. Since the distance from the loading force action line is small, the fracture is not prone to deflect. In contrast, the new fracture of the upper rock needs to migrate horizontally for a certain distance based on the deflection of the lower rock fracture and then expand upward. The distance from the loading force action line is significant, and the fracture is easy to deflect.

Comparing Fig. 10 and Fig. 5, it can be seen that the average deflection angle of the secondary mining fracture in the brittle rock is 1.8° and that in the plastic rock is 7.2°. When

the secondary mining fracture expands from brittle rock to the plastic rock, the average deflection angle in the brittle rock is 16.2°, and that in the plastic rock is 26.0°. When the secondary mining fracture expands from the plastic rock to the brittle rock, the average deflection angle in the plastic rock is 5.2°, and that in the brittle rock is 11.2°. The above data show that when the secondary mining fractures expand from brittle rock to plastic rock, the deflection angle of fractures in both rocks will increase. When the secondary mining fracture expands from plastic rock to brittle rock, the fracture propagation characteristics of the two will be neutralised, increasing the fracture deflection angle of the brittle rock and a decrease in the fracture deflection angle of the plastic rock.

4.3. Secondary mining failure behaviour and energy characteristics of combined rock,

The corresponding relationship between the cumulative acoustic emission count, absolute energy and load of the combined rock under three-point bending is shown in Figs. 11 to 14.

Fig. 11 shows that during the loading process of limestone-mudstone composite rock, the cumulative acoustic emission count before peak load continues to increase to 3.2×10^3. At the peak load, the fracture expands to the upper mudstone instantaneously, and the acoustic emission signal is strong. The cumulative acoustic emission count increases by 5.2×10^3, and the absolute energy released is 3.2×10^9 aJ, accounting for 99% of the total energy released. After peak load, with the expansion of the fracture, the cumulative acoustic emission count continues to rise. When the combined rock is destroyed, the cumulative acoustic emission count reaches the maximum, and the maximum value is 1.3×10^4.

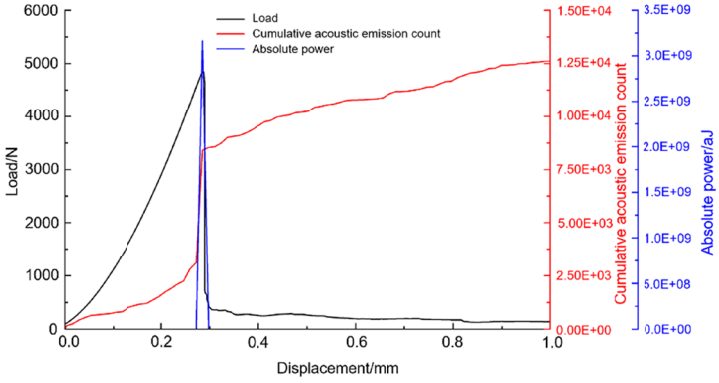

Fig. 11. Limestone-mudstone three-point bending 'load-cumulative acoustic emission count-absolute energy-displacement' curve diagram

Comparing Fig. 7, Fig. 8 and Fig. 11, it can be seen that the peak strength of limestone-mudstone composite rock is lower than that of limestone and mudstone. The damage degree of composite rock in the failure process is between that of two kinds of single rock. In the whole process of loading, there are internal micro-fractures, which have a certain energy absorption effect in the early stage of loading. The acoustic emission count growth and absolute energy

release of composite rock are the largest at the peak load, and a certain degree of damage can still occur after the peak load.

Fig. 12 shows that during the loading process of mudstone-fine sandstone combined rock, the cumulative acoustic emission count continued to increase before the first peak load. At the first peak load, the fractures expand instantaneously in the mudstone, and the acoustic emission signal is strong. The cumulative acoustic emission count increases by 5.2×10^3, and the absolute energy released is 8.2×10^8 aJ, accounting for 76% of the total energy released. After the first peak load, the fracture continued to expand upward to the rock interface and then underwent horizontal migration. The cumulative acoustic emission count continued to rise. At the second peak load, the fracture passes through the interface and expands instantaneously in the fine sandstone. The acoustic emission signal is strong, the acoustic emission count increases by 1.5×10^3, and the absolute energy released is 2.6×10^8 aJ. After the peak load, with the expansion of the fracture, the cumulative acoustic emission count continues to rise. When the combined rock is destroyed, the cumulative acoustic emission count reaches the maximum, and the maximum value is 1.3×10^4.

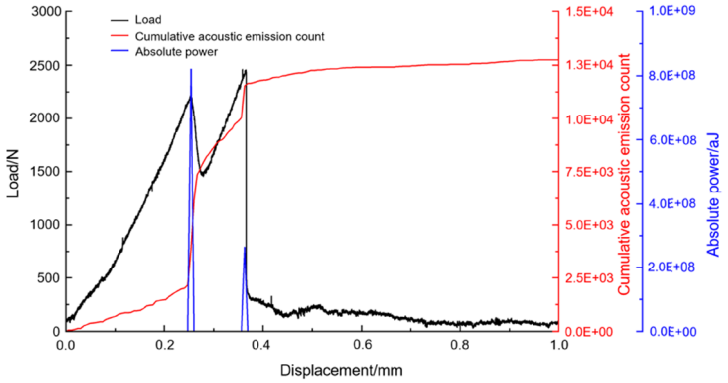

Fig. 12. Mudstone-fine sandstone three-point bending 'load-cumulative acoustic emission count-absolute energy-displacement' curve diagram

By comparing Fig. 6, Fig. 8 and Fig. 12, it can be seen that the peak strength of mudstone-fine sandstone combined rock is lower than that of mudstone and fine sandstone. The damage degree of the combined rock during the failure process is between the two kinds of single rock. It produces a lot of damage and releases energy at the two peak loads. In the second increase stage of the load, the fractures expand horizontally at the interface of the two kinds of rocks, and the acoustic emission count continues to rise, but the absolute energy is not significantly increased. After the second peak load, the fractures enter the fine sandstone, and the micro-fracture generation rate slows down.

Fig. 13 shows that the cumulative acoustic emission count continues to increase before the fine sandstone-mudstone composite rock reaches the first peak load. At the first peak load, the fracture expands instantaneously in the fine sandstone, and the acoustic emission signal is strong. The cumulative acoustic emission count increases by 1.1×10^3, and the absolute energy released is 7.2×10^7 aJ. After reaching the first peak load, the fracture continues to expand upward to the rock interface and then undergoes horizontal migration, and the cumulative acoustic emis-

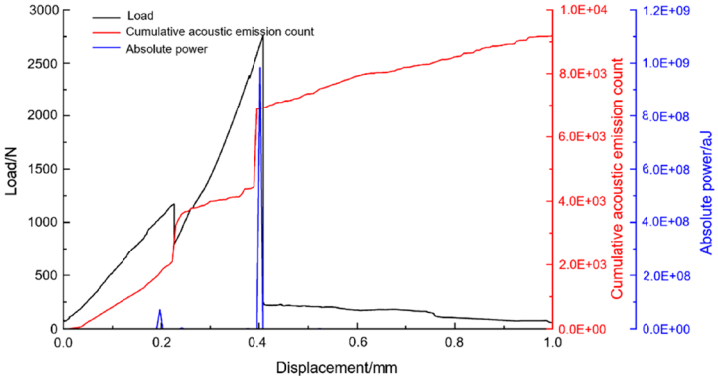

Fig. 13. Three-point bending 'load-cumulative acoustic emission count-absolute energy-displacement' curve of fine sandstone-mudstone

sion count increases slowly. At the second peak load, the fracture expands instantaneously in the mudstone through the interface, and the acoustic emission signal is strong. The cumulative acoustic emission count increases by 2.4×10^3, and the absolute energy released is 9.8×10^8 aJ, accounting for 92% of the total energy released. After the peak load, with the expansion of the fracture, the cumulative acoustic emission count continues to rise. When the combined rock is destroyed, the cumulative acoustic emission count reaches the maximum, with a maximum value of 9.3×10^3.

By comparing Fig. 6, Fig. 8 and Fig. 13, it can be seen that the peak strength of the fine sandstone-mudstone combined rock is lower than that of the fine sandstone and mudstone. The damage degree of the combined rock during the failure process is between the two single rocks. It produces a large amount of damage and releases energy at the two peak loads. In the second load increase stage, the fractures expand horizontally at the interface of the two rocks, and the acoustic emission count continues to rise, but the absolute energy is not significantly increased. After the second peak load, the fractures enter the mudstone, and the rock damage still increases at a relatively rapid rate.

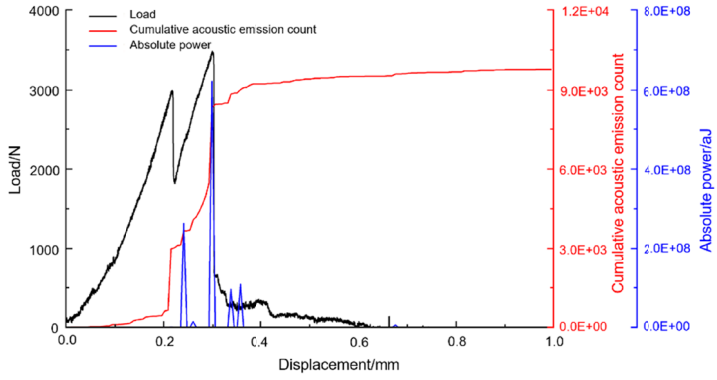

Fig. 14. Mudstone-limestone three-point bending 'load-cumulative acoustic emission count-absolute energy-displacement' curve diagram

Fig. 14 shows that during the loading process of mudstone-limestone combined rock, the cumulative acoustic emission count continued to increase before the first peak load. At the first peak load, the fractures expand instantaneously in the mudstone, and the acoustic emission signal is strong. The cumulative acoustic emission count increases by 2.4×10^3, and the absolute energy released is 2.6×10^8 aJ. Between the first peak load and the second peak load, the fractures migrate horizontally at the rock interface, and the acoustic emission signal is relatively strong at this time. At the second peak load, the fracture expands into the limestone, and the acoustic emission signal is enhanced again. The cumulative acoustic emission count increases by 2.9×10^3, and the absolute energy released is 6.2×10^8 aJ, accounting for 54% of the total energy released. After the peak load, with the expansion of the fracture, the cumulative acoustic emission count continues to rise ; when the combined rock is completely destroyed, the cumulative acoustic emission count reaches the maximum, with a maximum value of 9.7×10^3.

Comparing Fig. 7, Fig. 8 and Fig. 14, it can be seen that the peak strength of mudstone-limestone composite rock is lower than that of mudstone and limestone. The damage degree of composite rock during failure is between that of two kinds of single rock. It produces a lot of damage and releases energy at two peak loads. When the fracture expands at the horizontal interface, the cumulative acoustic emission count grows fastest, and there is a weak absolute energy release.

By comparing and analysing Figs. 6-8 and Figs. 11-14, the following rules can be obtained:

(1) For the combined rock composed of different strength rocks, the change of acoustic emission count is consistent: the acoustic emission count increases linearly before reaching the peak load, increases sharply when reaching the peak load, and increases slowly with the growth of fractures in the process of peak load to complete rock failure.

(2) For the composite roof composed of different strength rocks, the damage degree in the failure process is between the two kinds of single rock. The damage increases rapidly when the fracture expands in the two kinds of rock strata, and the damage degree slows down when the fracture migrates horizontally at the interface of the composite roof.

(3) The energy released by the fracture of the composite roof mainly depends on the high-strength roof. The energy released by the fracture of the high-strength roof is higher than that released by the fracture of the low-strength roof. The process of horizontal migration of fissures at the interface of composite roof hardly releases energy.

(4) When the strength of the lower rock of the composite roof is much larger than that of the upper rock, the energy release during the failure process is similar to that of the lower high- strength rock. The energy release is very concentrated, and the peak energy release accounts for more than 90% of the total.

5. Conclusions

(1) The characteristics of secondary mining-induced fracture propagation in the roof are as follows: When the fracture extends from a brittle roof to a plastic roof, the deflection angle of the fracture in the two roofs increases. When the fracture extends from a plastic roof to a brittle roof, the fracture propagation characteristics of the two will be neutralised. Under the action of secondary mining, the higher the tensile strength of the brittle roof is, the smaller the deflection amplitude of secondary mining fracture propagation is. The deflection amplitude of the secondary mining fracture of the plastic roof is larger than that of a brittle roof. When the fracture propagates in the composite roof

composed of different strength rocks, the deflection angle in the lower roof is smaller than that in the upper roof, and the overall deflection angle difference between the two roofs is about 8°.

(2) The damage and failure law of secondary mining fractures in the inner layer of the roof is as follows: The failure process of the brittle roof is short, and there are many damages in the failure process. The failure process of the plastic roof is long, with less damage in the process and a more moderate failure process. The stronger the bearing capacity of the brittle roof, the more internal damage there is and the more thorough the damage. For the composite rock mass, its peak load is less than the peak load of the single rock mass which is composed of it, and the damage degree during the failure process is between the two single rocks. The damage increases rapidly at the moment of fracture propagation in the two rock layers, and the growth rate of the damage degree slows down when the fracture propagates at the interface of the composite roof.

(3) The energy evolution of the secondary mining fracture in the roof has the following rules: The energy released by the brittle rock roof during the final fracture is the largest, and the plastic rock roof releases the most energy at the moment of fracture. The higher the tensile strength of a brittle roof, the more energy is released during the fracture process, and the energy released during the fracture process of the brittle roof is higher than that released during the fracture process of a plastic roof. The energy released by the fracture of the composite roof mainly depends on the high-strength roof. The energy released by the fracture of the high-strength roof is higher than that released by the fracture of the low-strength roof. The process of horizontal migration of the fracture at the interface of the composite roof hardly releases energy.

Acknowledgments

The work is funded by the Basic Research Foundation of Shanxi Province, China (Grant No. 202303021221007) and National Natural Science Foundation of China (Grant No.U22A20167).

References

[1] Guoshu Yang, Jianshu Wang, Overburden structure evolution and pressure law of second mining in a close-range coal seam group. Journal of China Coal Society **43** (2), 353-358 (2018). DOI: https://doi.org/10.13225/j.cnki.jccs.2018.1616

[2] Xuping Li, Yanqing Liu, Xiaopeng Ren, et al., Roof breaking characteristics and mining pressure APPEARANCE laws in close distance COAL seams. Energy Exploration & Exploitation **41** (2), 728-744 (2023). DOI: https://doi.org/10.1177/01445987221120888

[3] Qingxiang Huang, Jinbo Han, Study on fracture evolution mechanism of shallow-buried close coal seam mining. Journal of Mining & Safety Engineering **36** (4), 706-711 (2019). DOI: https://doi.org/10.13545/j.cnki.jmse.2019.04.008

[4] Dengyun Hao, Yongzheng Wu, Haijun Chen, et al., Instability mechanism and prevention technology of roadway in close distance and extra thick coal seam under goaf. Journal of China Coal Society **44** (9), 2682-2690 (2019). DOI: https://doi.org/10.13225/j.cnki.jccs.2019.0217

[5] Hongbao Zhao, Hui Cheng, Dongliang Ji, et al., Study of the mechanism and evolution law of unsymmetrical failure of the mining roadway in close distance coal seam. Journal of China University of Mining & Technology **50** (6), 1029-1040+1050 (2021). DOI: https://doi.org/10.13247/ j.cnki.jcumt.001342

[6] Hongpu Kang, Pengfei Jiang, Bingxiang Huang, et al., Roadway strata control technology by means of bolting-modification-destressing in synergy in 1000 m deep coal mines. Journal of China Coal Society **45** (3), 845-864 (2020). DOI: https://doi.org/10.13225/j.cnki.jccs.SJ20. 0204

[7] Yaming Zhao, Wei Yang, Yang Chen, Spontaneous combustion prevention technology of withdrawal working face of spontaneous combustion thick coal seam in rock burst mine. Safety in Coal Mines **53** (4), 81-86+93 (2022). DOI: https://doi.org/10.13347/j.cnki.mkaq.2022.04.013

[8] Zhenqi Liu, Xiaoxing Zhong, et al., Redevelopment of Fractures and Permeability Changes after Multi-Seam Mining of Shallow Closely Spaced Coal Seams. Archives of Mining Sciences **67** (4), 681-697 (2022). DOI: https://doi.org/10.24425/ams.2022.143681

[9] Yangquan Jiao, Shuangming Wang, Limin Fan, et al., Key elements and framework model of groundwater system in Jurassic coal measures of Ordos Basin. Journal of China Coal Society **45** (7), 2411-2422 (2020). DOI: https://doi.org/10.13225/j.cnki.jccs.dz20.0930

[10] Minggao Qian, Xiexing Miao, Fulian He, Key block analysis of 'masonry beam' structure in stope. Journal of China Coal Society 1994 (06), 557-563 (1994).

[11] Wei Wang, Zhongbiao Gong, Deformation law and control of surrounding rock of dynamic pressure roadway under coal pillar in close seam group. Coal Science and Technology **50** (2), 143-152 (2022). DOI: https://doi.org/10.13199/j.cnki.cst.2022-2089.

[12] Dawei Yin, Shaojie Chen, et al, Simulation Study on Strength and Failure Characteristics of Coal-Rock Composite Sample with Coal Persistent Joint. Archives of Mining Sciences **64** (3), 609-623 (2019). DOI: https://doi.org/10.24425/ams.2019.129372

[13] Jisheng Xue, Tielin Zhao, Deformation and Fracture Characteristics of Coal Gangue Interbedded Samples under Loading and Unloading Conditions. Advances in Civil Engineering. (2022). DOI: https://doi.org/10.1155/2022/7734078

[14] Susheng Wang, Shengqi Yang, Wenling Tian, et al., Research on phase-field simulation method of crack propagation of rock with pre-existing fissures. Chinese Journal of Rock Mechanics and Engineering **42** (2), 365-377 (2023). DOI: https://doi.org/10.13722/j.cnki.jrme.2022. 0267

[15] Qi Li, Zhen Li, Peng Li, et al., Analysis on meso-deformation and fracture evolution features of coal based on CT scanning under in-situ loading. Mining Research and Development **43** (4), 110-115 (2023). DOI: https://doi.org/10.13827/j.cnki.kyyk.2023.04.012

[16] Jie Zhang, Yifeng He, Nan Luo, et al., Research on overburden movement and fracture evolution of repeated mining in shallow coal seams group. Safety in Coal Mines **53** (3), 58-65 (2022). DOI: https://doi.org/10.13347/j.cnki.mkaq.2022.03.010

[17] Jianhua Li, Shuai Wang, Yanjun He, et al., Fissure evolution of gob overlying strata under superimposed mining in coal seams group. Coal Engineering **53** (12), 92-96 (2021).

[18] Ping Cao, Taoying Liu, Chengzhi Pu, et al., Crack propagation and coalescence of brittle rock-like specimens with pre-existing cracks in compression. Engineering Geology **187**, 113-121 (2015). DOI: https://doi.org/10.1016/j.enggeo.2014.12.010

[19] Yizhao Wang, Zhendong Cui, Ming Li, et al., Effect of layer thickness of flaggy rock on crack propagation path subjected to three-point bending. Journal of Engineering Geology **26** (5), 1326-1335 (2018). DOI: https://doi.org/10.13544/j.cnki.jeg.2018182

[20] Yingming Yang, Zhibo Ma, Weilong Zhang, et al., Study on crack propagation in layered rock under the three-point bending conditions. Frontiers in Earth Science (2023). DOI: https://doi.org/10.3389/feart.2022.1084272

[21] Kezhong Wang, Chun Zhang, Yaohui Gao, et al., Influence of Prefabricated Fissure Combinations on Strength and Failure Characteristics of Rock-Like Specimens under Uniaxial Compression. International Journal of Geomechanics **23** (2), (2023). DOI: https://doi.org/10.1061 /(asce)gm.1943-5622.0002637

[22] Xiaoyi Chen, Study on crack propagation behavior and mechanical characteristics of composite roof of rectangular. Inner Mongolia University of Science & Technology (2022). DOI: https://doi.org/10.27724/d.cnki.gnmgk.2022.000401

[23] Zhijian Lin, Research on Mechanical Properties and Crack Propagation Characteristics of Layered Sandstone Under Three-point Bending Conditions. North China University of Water Resources and Electric Power (2022). DOI: https://doi.org/10.27144/d.cnki.ghbsc.2022.000499